

The Dramatic Effect of Architecture on the Self-Assembly of Block Copolymers at Interfaces

Yoojin Kim,^{†,||} Jeffrey Pyun,^{‡,§,||} Jean M. J. Fréchet,^{§,||} Craig J. Hawker,^{‡,||} and Curtis W. Frank^{*,†,||}

Department of Chemical Engineering, Stanford University, Stanford, California 94305-5025, IBM Almaden Research Center, 650 Harry Road, San Jose, California 95120-6001, Center for New Directions in Organic Synthesis, Department of Chemistry, University of California, Berkeley, California 94720-1460, and Center on Polymer Interfaces and Macromolecular Assemblies, IBM Almaden Research Center, San Jose, California 95120

Received November 23, 2004. In Final Form: February 18, 2005

Dramatic morphological changes are observed in the Langmuir–Blodgett (LB) film assemblies of poly(ethylene glycol)-*b*-(styrene-*r*-benzocyclobutene) block copolymer (PEG-*b*-(S-*r*-BCB)) after intramolecular cross-linking of the S-*r*-BCB block to form a linear-nanoparticle structure. To isolate architectural effects and allow direct comparison, the linear block copolymer precursor and the linear-nanoparticle block copolymer resulting from selective intramolecular cross-linking of the BCB units were designed to have exactly the same molecular weight and chemical composition but different architecture. It was found that the effect of architecture is pronounced with these macromolecular isomers, which self-assemble into dramatically different surface aggregates. The linear block copolymer forms disklike surface assemblies over the range of compression states, while the linear-nanoparticle block copolymer exhibits long (> 10 μm) wormlike aggregates whose length increases as a function of increasing cross-linking density. It is shown that the driving force behind the morphological change is a combination of the altered molecular geometry and the restricted degree of stretching of the nanoparticle block because of the intramolecular cross-linking. A modified approach to interpret the π -A isotherm, which includes presence of the block copolymer aggregates, is also presented, while the surface rheological properties of the block copolymers at the air–water interface provide in-situ evidence of the aggregates' presence at the air–water interface.

Introduction

One of the most fascinating properties of block copolymers is their ability to self-assemble into micelles, aggregates, and vesicles of various morphologies in the presence of a selective solvent,^{1–3} and recent studies have demonstrated that self-assembly of block copolymers into various morphologies occurs not only in selective solvents but also at interfaces and surfaces.^{4,5} In the case of amphiphilic or surface-adsorbing block copolymers, the self-assembled structure at the air–water interface can also be transferred to a solid substrate using the Langmuir–Blodgett (LB) transfer technique.^{6–22} Thin block

copolymer films with nanometer-scale order have received much attention, driven by their prospective applications as lithographic masks,²³ photonic materials,²⁴ and nano-patterned substrates for microelectronics²⁵ and in biomedical devices.^{26,27} While these previous studies have concentrated primarily on the self-assembly of amphiphilic, linear diblock, and triblock materials, significant advances have recently been made in the field of polymer synthesis, allowing access to block copolymers composed

* To whom correspondence should be addressed. E-mail curt.frank@stanford.edu.

[†] Stanford University.

[‡] IBM Almaden Research Center.

[§] University of California.

^{||} Center on Polymer Interfaces and Macromolecular Assemblies.

(1) Ma, Q.; Remsen, E. E.; Clark, C. G.; Kowalewski, T.; Wooley, K. L. *Proc. Natl. Acad. Sci.* **2002**, *99*, 5058–5066.

(2) Hubbell, J. A. *Science* **2003**, *300*, 595–596.

(3) Pochan, D. J.; Chen, Z.; Cui, H.; Hales, K.; Oi, K.; Wooley, K. L. *Science* **2004**, *306*, 94–97.

(4) Mezzenga, R.; Ruokolainen, J.; Fredrickson, G. H.; Kramer, E. J.; Moses, D.; Heeger, A. J.; Ikkala, O. *Science* **2003**, *299*, 1872–1874.

(5) Russell, T. P. *Science* **2002**, *297*, 964–967.

(6) Zhu, J. Y.; Eisenberg, A.; Lennox, R. B. *J. Am. Chem. Soc.* **1991**, *113*, 5583–5588.

(7) Zhu, J.; Hanley, S.; Eisenberg, A.; Lennox, R. B. *Makromol. Chem. Macromol. Symp.* **1992**, *53*, 211–220.

(8) Zhu, J. Y.; Lennox, R. B.; Eisenberg, A. *J. Phys. Chem.* **1992**, *96*, 4727–4730.

(9) Cox, J. K.; Yu, K.; Constantine, B.; Eisenberg, A.; Lennox, R. B. *Langmuir* **1999**, *15*, 7714–7718.

(10) Cox, J. K.; Yu, K.; Eisenberg, A.; Lennox, R. B. *Phys. Chem. Chem. Phys.* **1999**, *1*, 4417–4421.

(11) Baker, S. M.; Leach, K. A.; Devereaux, C. E.; Gragson, D. E. *Macromolecules* **2000**, *33*, 5432–5436.

(12) Devereaux, C. A.; Baker, S. M. *Macromolecules* **2002**, *35*, 1921–1927.

(13) Kumaki, J.; Hashimoto, T. *J. Am. Chem. Soc.* **1998**, *120*, 423–424.

(14) Li, S.; Hanley, S.; Khan, I.; Varshney, S. K.; Eisenberg, A.; Lennox, R. B. *Langmuir* **1993**, *9*, 2243–2246.

(15) Li, S.; Clarke, C. J.; Lennox, R. B.; Eisenberg, A. *Colloids Surf., A* **1998**, *133*, 191–203.

(16) Li, S.; Clarke, C. J.; Eisenberg, A.; Lennox, R. B. *Thin Solid Films* **1999**, *354*, 136–141.

(17) Meszaros, M.; Eisenberg, A.; Lennox, R. B. *Faraday Discuss.* **1994**, 283–294.

(18) Seo, Y.; Im, J.-H.; Lee, J.-S.; Kim, J.-H. *Macromolecules* **2001**, *34*, 4842–4851.

(19) Seo, Y.; Paeng, K.; Park, S. *Macromolecules* **2001**, *34*, 8735–8744.

(20) Seo, Y.; Esker, A. R.; Sohn, D.; Kim, H.-J.; Park, S.; Yu, H. *Langmuir* **2003**, *19*, 3313–3322.

(21) Xu, H.; Erhardt, R.; Abetz, V.; Muller, A. H. E.; Goedel, W. A. *Langmuir* **2001**, *17*, 6787–6793.

(22) Francis, R.; Skolnik, A. M.; Carino, S. R.; Logan, J. L.; Underhill, R. S.; Angot, S.; Taton, D.; Gnanou, Y.; Duran, R. S. *Macromolecules* **2002**, *35*, 6483–6485.

(23) Park, M.; Harrison, C.; Chaikin, P. M.; Register, R. A.; Adamson, D. H. *Science* **1997**, *276*, 1401.

(24) Fink, Y.; Urbas, A. M.; Bawendi, M. G.; Joannopoulos, J. D.; Thomas, E. L. *J. Lightwave Technol.* **1999**, *17*, 1963–1969.

(25) Kim, S. O.; Solak, H. H.; Stoykovich, M. P.; Ferrier, N. J.; de Pablo, J. J.; Nealey, P. F. *Nature* **2003**, *424*, 411–414.

(26) Otsuka, H.; Nagasaki, Y.; Kataoka, K. *Curr. Opin. Colloid Interface Sci.* **2001**, *6*, 3–10.

(27) Tokuhisa, H.; Hammond, P. T. *Langmuir* **2004**, *20*, 1436–1441.

of a variety of complex architectures. Micelles arising from star^{28–30} and cyclic block copolymers,^{31,32} Janus micelles,^{21,33} as well as the aggregation of dendritic-linear block copolymers³⁴ and the self-assembly of monodendron-jacketed polymers³⁵ have been reported. In this paper, the effect of macromolecular architecture on the self-assembly process of isomeric block copolymers and the resulting effect on morphologies are examined. This allows the role of architecture to be systematically studied and provides a unique opportunity to explore the underlying relationship between the three-dimensional structure and the physical properties of the molecules and their self-assembly process.

To investigate these issues, the interfacial self-assembly of a new hybrid poly(ethylene glycol-*b*-(styrene-*r*-benzocyclobutene)) block copolymer (PEG-*b*-(S-*r*-BCB)) in which both architectural and polarity differences exist between the blocks was examined. The linear PEG block is surface active at the air–water interface, while the hydrophobic S-*r*-BCB block, acting as a buoy at the interface, is intramolecularly cross-linked to yield a nanoparticle architecture.³⁶ The results are compared with data on the linear block copolymer. The linear block copolymer precursor and the linear-nanoparticle block copolymer resulting from selective intramolecular cross-linking of the BCB units have the same chemical composition and overall molecular weight, thus providing a straightforward comparison of the effect of architecture. In addition, variations in the cross-linking density of the hydrophobic nanoparticle block allow detection of the morphological transition caused by the architectural changes as a function of cross-linking density.

In this manuscript, the concept of architectural isomers in block copolymers and its relation to self-assembly was examined by the initial synthesis and bulk characterization of PEG-*b*-(S-*r*-BCB) isomers. The π -*A* isotherms, viscoelastic measurements, and AFM images of the LB films of these amphiphilic systems are then used to characterize the interfacial properties of the block copolymers. These studies allow a rationale for the remarkable morphological difference in the self-assembly and surface aggregates of the block copolymers, which differ only in their macromolecular architecture, to be proposed.

Experimental Section

Diblock Copolymer Synthesis. General Methods. The apparent molecular weights and polydispersities of polymer samples were analyzed by gel permeation chromatography performed in tetrahydrofuran (THF) on a Waters chromatograph equipped with four 5- μ m Waters columns (300 mm \times 7.8 mm) connected in series with increasing pore size (100, 1000, 100 000, 1 000 000 Å). A Waters 410

differential refractometer and a 996-photodiode-array detector were employed. Linear polystyrene standards and poly(ethylene glycol) standards were used to calibrate the retention time and to calculate the molecular weight. The GPC results were used to compare the bulk structural characteristics of the linear vs linear-nanoparticle block copolymers. ¹H and ¹³C nuclear magnetic resonance spectra were obtained on a Bruker AVANCE 400 FT-NMR spectrometer using deuterated chloroform as a solvent in all samples.

Methyl(2,2,5-trimethyl-3-(benzylethoxy)-4-phenyl-3-azahexane)poly(ethylene glycol), **3**. NaH (0.05 g, 1.25 mmol) was slowly added to a mixture of monomethylpoly(ethylene glycol), **1** (5.00 g, 0.25 mmol), and 18-crown-6 (10 mg) dissolved in 10 mL dry THF under a constant argon flow. After 15 min, the chloromethyl-substituted alkoxyamine, **2** (0.37 g, 1.00 mmol),³⁷ was added to the reaction mixture, which was subsequently heated at reflux for 16 h. After the addition of a few drops of water to neutralize the excess NaH, the reaction mixture was concentrated and dissolved in dichloromethane. The crude product was obtained after two precipitation steps into diethyl ether to give the PEG-macroinitiator, **3**, as a colorless solid (4.71 g, 92.3%); IR (KBr): 3439 cm⁻¹ (NH), 1693 cm⁻¹ (amide). ¹H NMR (400 MHz, CDCl₃) δ 7.4–7.1 (m, ArH), 4.96 (d, CH), 4.60 (d, CH₂OAr), 3.65 (s, OCH₂), 3.45 (d, CH), 3.32 (d, CH), 2.38 (m, CH), 1.65 (d, CH₃), 1.52 (d, CH₃), 1.40 (m, CH), 1.33 (d, CH₃), 1.05 (s, *t*-Bu), 0.89 (d, CH₃), 0.80 (s, *t*-Bu), 0.61 (d, CH₃), and 0.22 (d, CH₃).

*Poly(ethylene glycol)-b-(styrene-*r*-benzocyclobutene)*, **5**. The poly(ethylene glycol) terminated alkoxyamine, **3** (500 mg, 0.025 mmol) ($M_n = 20\ 000$, PDI = 1.07), was dissolved in styrene (1.65 g, 15.85 mmol) and 4-vinylbenzocyclobutene, **4** (0.364 g, 2.80 mmol),³⁶ in a glass ampule with a stir bar. After three freeze-and-thaw cycles, the ampule was sealed under argon and was heated for 5 h at 120 °C. The resulting polymer was dissolved in THF and was purified by precipitation into deionized water followed by reprecipitation into hexane. Further purification to remove p(S-*r*-BCB) contamination was performed by multiple extractions with cyclohexane at 35 °C to give **5** as a colorless powder (1.30 g, 52%), $M_w = 79\ 600$; PDI = 1.17; ¹H NMR (400 MHz, CDCl₃) δ : 7.24–6.57 (m, ArH), 3.65 (s, OCH₂), 3.05 (br s, CH₂), 1.83–1.26 (m, CH₂, CH).

Linear-Nanoparticle Block Copolymer Formation, **6**. In a 500 mL three-necked flask equipped with an internal thermometer and septum, 200 mL of dibenzyl ether was first purged with argon and was heated at 250 °C under argon. A solution of the BCB-functionalized linear block copolymer, **5** (100 mg, $M_w = 79\ 600$; PDI = 1.17, 15 mol % BCB), dissolved in dibenzyl ether (100 mL) was added dropwise via a peristaltic pump at ca. 20.0 mL/h with vigorous stirring under argon. After addition, the reaction mixture was heated for an additional 1 h, the solvent was distilled under reduced pressure, and the remaining crude product was dissolved in dichloromethane and was precipitated into hexane twice. This gave the linear-nanoparticle block copolymer, **6**, as a colorless solid (78 mg, 78% yield, $M_w = 35\ 200$; PDI = 1.18), ¹H NMR (400 MHz, CDCl₃). The significant change in the ¹H NMR was the disappearance of the aliphatic benzocyclobutene protons at 3.05 ppm upon formation of the cross-linked nanoparticles; all other aspects of the spectrum were similar.

Thermal Characterization in Bulk. A TA Instruments Q1000 modulated differential scanning calorimeter (mDSC) was used to study the thermal behavior of the

(28) Pispas, S.; Hadjichristidis, N.; Potemkin, I.; Khokhlov, A. *Macromolecules* **2000**, *33*, 1741–1746.

(29) Djalali, R.; Hugenberg, N.; Fischer, K.; Schmidt, M. *Macromol. Rapid Commun.* **1999**, *20*, 444–449.

(30) Iatrou, H.; Willner, L.; Hadjichristidis, N.; Halperin, A.; Richter, D. *Macromolecules* **1996**, *29*, 581–591.

(31) Borsali, R.; Minatti, E.; Putaux, J.-L.; Schappacher, M.; Deffieux, A.; Viville, P.; Lazzaroni, R.; Narayanan, T. *Langmuir* **2003**, *19*, 6–9.

(32) Minatti, E.; Viville, P.; Borsali, R.; Schappacher, M.; Deffieux, A.; Lazzaroni, R. *Macromolecules* **2003**, *36*, 4125–4133.

(33) Erhardt, R.; Böker, A.; Zettl, H.; Kaya, H.; Pyckhout-Hintzen, W.; Krausch, G.; Abetz, V.; Müller, A. H. E. *Macromolecules* **2001**, *34*, 1069–1075.

(34) van Hest, J. C. M.; Delnoye, D. A. P.; Baars, M. W. P. L.; van Genderen, M. H. P.; Meijer, E. W. *Science* **1995**, *268*, 1592–1595.

(35) Percec, V.; Ahn, C.-H.; Ungar, G.; Yeardley, D. S. P.; Moller, M.; Sheiko, S. S. *Nature* **1998**, *391*, 161–164.

(36) Harth, E.; Van Horn, B.; Lee, V. Y.; Germack, D. S.; Gonzales, C. P.; Miller, R. D.; Hawker, C. J. *J. Am. Chem. Soc.* **2002**, *124*, 8653–8660.

(37) Hawker, C. J. *J. Am. Chem. Soc.* **1994**, *116*, 11185–11186.

polymer samples. The samples were heated at a constant rate of 10 °C per minute with a modulation of ± 0.5 °C per 20 s. Four runs were taken for the linear block copolymers with the following temperature changes: run 1, $-40\sim 170$ °C; run 2, $-40\sim 170$ °C; run 3, $-40\sim 300$ °C; and run 4, $-40\sim 170$ °C. The first run was performed to remove the thermal history of the polymer, and the third and fourth runs were performed to promote the cross-linking reaction of the BCB units and to determine the influence of intermolecular cross-linking, respectively. Two runs from -40 to 170 °C were taken for the linear-nanoparticle block copolymers; the first run was to remove the thermal history of the polymer and the second run was to investigate the effect of intramolecular cross-linking. The error in the melting point and glass-transition measurements was ± 2 °C.

Surface Pressure–Area (π -A) Isotherm and Langmuir–Blodgett Film Transfer. Solutions of the copolymers were prepared in spectroscopic grade chloroform (J. T. Baker) with a concentration of 1.0 ± 0.1 mg/mL. A $50\text{ cm} \times 15\text{ cm}$ symmetric-compression KSV5000 Langmuir–Blodgett trough (KSV, Helsinki) was used for the π -A isotherm measurements and LB film transfers in a temperature-controlled class 1000 clean room. The surface pressure was measured using the Wilhelmy plate method with a rectangular platinum plate. The subphase was deionized water purified with a Milli-Q system (Millipore Corp.) to $18.2\text{ M}\Omega\text{-cm}$ resistivity. The subphase water temperature was maintained at 25.0 ± 0.1 °C. In a typical experiment, $25\text{--}120\ \mu\text{L}$ of the polymer solution was spread in small drops on the water surface using a Hamilton microsyringe. After solvent evaporation (15–20 min), the barriers were compressed at a constant rate, and the π -A isotherm was recorded. Each compression isotherm was composed of two parts because the trough only allowed one order-of-magnitude area compression factor. The isotherms obtained from the two compressions matched each other well for all the samples.

For an LB transfer, a $2\text{ cm} \times 3\text{ cm}$ n-type Si(100) wafer polished on both sides and $425\text{--}500\ \mu\text{m}$ thick was first cleaned by sonication in Piranha solution (3:1 mixture of sulfuric acid and 30% hydrogen peroxide) followed by rinsing with deionized water. The clean substrate was then immersed in the subphase before the polymer solution was spread. After the desired surface pressure was reached, the substrate was slowly removed from the subphase, passing vertically through the interface and transferring the polymer layer at the air–water interface to the solid substrate while maintaining the surface pressure. The substrate withdrawal rate was typically 0.1 mm/min , which resulted in transfer ratios close to unity ($0.73\sim 0.99$) at surface pressures higher than the pseudoplateau pressure (at 15 and 25 mN/m). At lower surface pressures (below 8 mN/m), especially near the pseudoplateau region (at 8 mN/m), a large dilational creep was observed over a period of 1 h. This led to transfer ratios larger than unity ($1.47\sim 3.10$) for lower surface pressures. The LB films were dried overnight and AFM images were acquired with a NanoScope III multimode AFM in tapping mode (Digital Instruments) using an “E” scanner with a microfabricated silicon cantilever (thickness = $4.1\text{--}4.5\ \mu\text{m}$, width = $30\text{--}31\ \mu\text{m}$, length = $123\ \mu\text{m}$, tip height = $10\text{--}15\ \mu\text{m}$, resonance frequency = $346\text{--}386\text{ kHz}$, and spring constant = $46\text{--}64\text{ N/m}$, Nanosensors).

Interfacial Stress Rheometer. Viscoelastic properties of the block copolymers at the air–water interface were measured using an interfacial stress rheometer (ISR). The details of this instrument are found in an article by Brooks

et al.³⁸ A $32.3\text{ cm} \times 7.5\text{ cm}$ symmetric-compression KSV mini-Langmuir trough was used to compress the polymer at the air–water interface and to monitor the surface pressure. The experiment was performed in a temperature-controlled class 1000 clean room, and the spreading technique, surface pressure measurement, and temperature control were the same as described above for the π -A isotherm measurement.

A thin magnetic rod was placed in the center of two parallel glass channels located in the middle of the trough. The magnetic rod was stabilized at the interface by surface tension and was subjected to an oscillatory magnetic field gradient generated by a pair of Helmholtz coils. An inverted microscope and a linear photodiode array were employed to detect the position of the rod as a function of time. The amplitude and the phase of the sinusoidal oscillation of the end of the rod position were then recorded using LABVIEW (National Instruments). The dynamic surface shear modulus, G_s^* , was calculated from the strain (γ_s) measured by the rod position as a function of the sinusoidal stress (σ_s). To verify that the rheology was independent of the amount of deformation, the strain was varied at a constant frequency (1.0 rad/s) to find the linear regime, within which the measurements were taken.

Results

The choice of poly(styrene-*b*-ethylene oxide) (PS-PEO) was motivated by the large number of studies on this system and by the classical nature of the parent, amphiphilic block copolymer. This allows comparison with the materials examined in this study since the primary structural difference is the presence of the S-*r*-BCB block in place of the styrene block of the PS-PEO system. In earlier research concerning monolayers of PS-PEO at the air–water interface, the PS-PEO block copolymers were thought to form homogeneous films.^{39,40} As a consequence, the corresponding π -A isotherms were also interpreted in terms of individual molecular conformation changes. As for grafted polymers,^{41–43} the surface-active PEO chain was thought to transform its conformation from a pancake to a quasi-brush and to a brush state with increasing surface pressure.

In 1998, da Silva et al.⁴⁴ suggested the existence of PS-PEO surface aggregates that had been transferred from the starting solution to the air–water interface. Since this report, several studies^{9,11,12} have revealed that the LB transferred films of PS-PEO show various self-assembled morphologies depending on the amphiphilic balance between the ethylene oxide and the styrene units. As a result, Cox et al.⁹ suggested the need for reevaluation of the π -A isotherms in terms of the surface aggregates. However, no in-situ evidence of surface aggregation at the air–water interface is available for the PS-PEO system, and thus, it has been difficult to rule out the possibility that the LB transfer process itself may be the cause of the surface aggregation, although aggregate formation has been observed in a single droplet experiment¹² on a clean silicon wafer for predominantly hydro-

(38) Brooks, C. F.; Fuller, G. G.; Frank, C. W.; Robertson, C. R. *Langmuir* **1999**, *15*, 2450–2459.

(39) Bijsterbosch, H. D.; de Haan, V. O.; de Graaf, A. W.; Mellema, M.; Leermakers, F. A. M.; Cohen Stuart, M. A.; van Well, A. A. *Langmuir* **1995**, *11*, 4467–4473.

(40) da Silva, A. M. G.; Filipe, E. J. M.; d'Oliveira, J. M. R.; Martinho, J. M. G. *Langmuir* **1996**, *12*, 6547–6553.

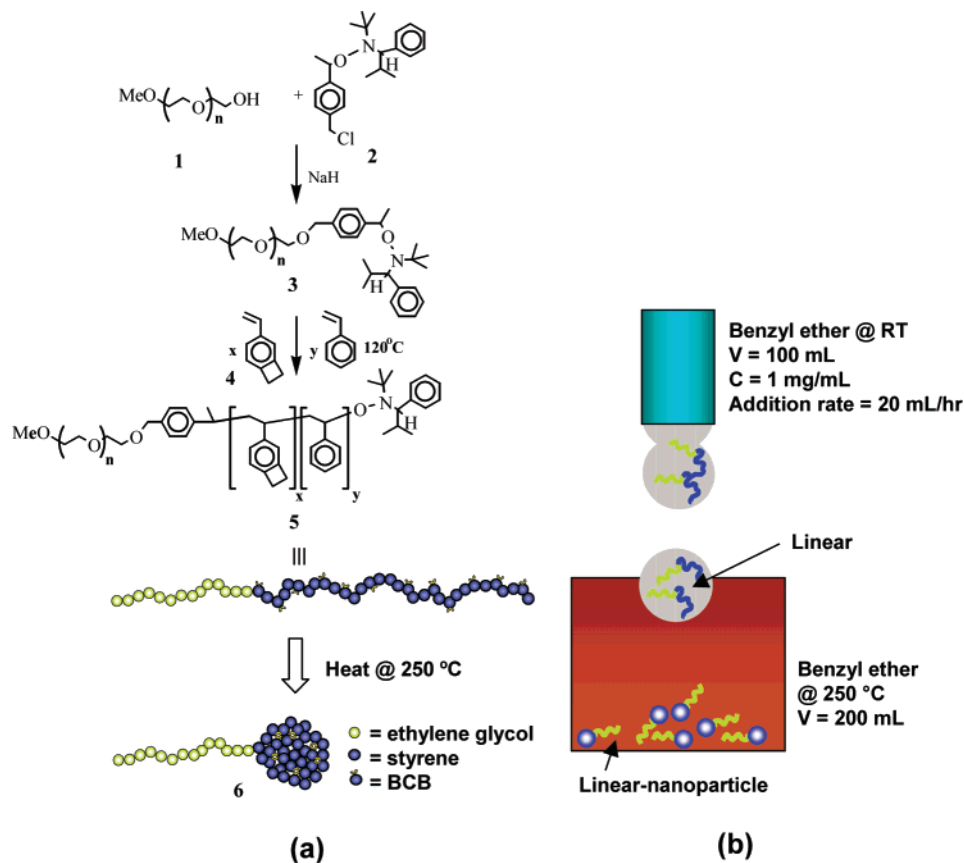
(41) Alexander, S. J. *Phys.* **1977**, *38*, 963.

(42) de Gennes, P. G. *Macromolecules* **1980**, *13*, 1069–1075.

(43) Ligoure, C. *J. Phys. II* **1993**, *3*, 1607–1617.

(44) da Silva, A. M. G.; Gamboa, A. L. S.; Martinho, J. M. G. *Langmuir* **1998**, *14*, 5327–5330.

Scheme 1. (a) Linear PEG-*b*-p(S-*r*-BCB) Block Copolymer Synthesis and Subsequent Cross-Linking of the S-*r*-BCB Block to Form the Linear-Nanoparticle Architecture and (b) the Typical Conditions for the Thermal Cross-Linking Reaction



phobic PS-PEO systems, which led to a proposed mechanism for competition between aggregation and solvent evaporation. Because of the lack of direct, in-situ information regarding the interfacial structures of the PS-PEO system at the air-water interface, the grafted polymer theory assuming individual molecules at the air-water interface is still largely adopted when interpreting the PS-PEO isotherm.⁴⁵ This theory applies to the region of the isotherm where the PS block occupies a significantly smaller area compared to the PEO block at the air-water interface, which is up to the pseudoplateau region shown for our linear system.

In this investigation of PEG-*b*-(S-*r*-BCB), the same question regarding the structure of the block copolymer at the air-water interface has been encountered: Does the block copolymer exist as individual molecules or as surface aggregates at the air-water interface? To answer this question, we have considered the surface viscoelastic properties of the block copolymers measured using the interfacial stress rheometer.³⁸ The result is interpreted under two scenarios in which (1) discrete molecules or (2) surface aggregates of the block copolymer exist at the air-water interface at different compression states.

Combining the surface dynamic moduli measurements with the morphologies of the LB transferred block copolymer films imaged by atomic force microscopy (AFM) as a function of different compression state, we use a modified approach to interpret the π -A isotherms of these amphiphilic block copolymers in which we took into account the presence of the surface aggregates at the air-water interface. We consider such interpretation more

appropriate for the block copolymers under study as we observe markedly different surface rheological behaviors between the linear and the linear-nanoparticle block copolymers, which could not be explained if the block copolymers existed as discrete molecules at the air-water interface. Although the focus of this study is on the morphological change of the surface aggregates promoted by the architectural difference of the macromolecules, it was essential to first establish that the surface aggregation process was occurring at the air-water interface rather than on the solid substrate after the LB transfer to understand how the different morphologies arise from the different block copolymer architectures.

Synthesis. To prepare the desired block copolymer, a recently developed method to build block copolymers with well-controlled hybrid architecture and synthesize architecturally defined nanoparticles via intramolecular chain collapse was employed.³⁶ The linear precursor and the linear-nanoparticle block copolymer are perfect analogues in terms of the overall molecular weight and chemical composition; they differ only in their architectures. Scheme 1 describes the synthesis procedure. Intramolecular chain collapse was achieved without the competing intermolecular cross-linking reaction by continuous addition of the linear precursor solution to hot benzyl ether at 250 °C, thus maintaining the concentration of the linear precursor in the solution low at all times. By varying the amount of the cross-linker (BCB) in the S-*r*-BCB block, we were able to make a series of block copolymers with unique linear-nanoparticle architecture in which the cross-linking density of the nanoparticle block is systematically controlled. Three linear-nanoparticle block copolymers containing 5, 10, and 15 mol % BCB in

(45) Rivillon, S.; Munoz, M. G.; Monroy, F.; Ortega, F.; Rubio, R. G. *Macromolecules* **2003**, *36*, 4068-4077.

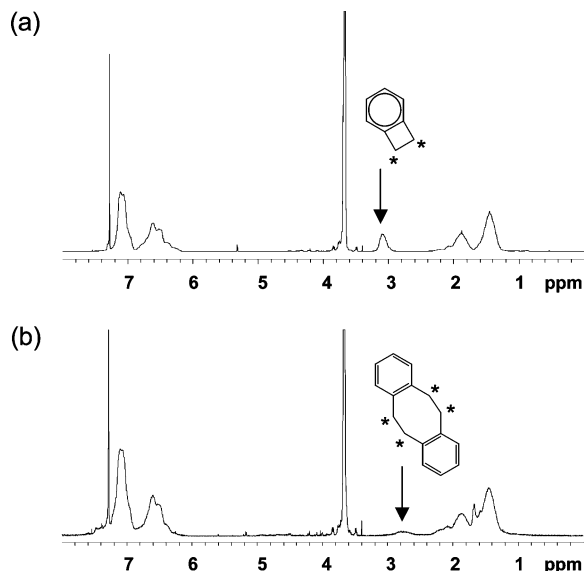


Figure 1. ^1H NMR of (a) the starting linear block copolymer with 15% BCB ($M_w = 79\,600$ g/mol, PDI = 1.17) and (b) the resulting linear-nanoparticle block copolymer after thermal treatment at $250\text{ }^\circ\text{C}$ (apparent $M_w = 35\,200$ g/mol, PDI = 1.18).

the S-*r*-BCB block and their linear precursors were synthesized and characterized.

^1H NMR was used to confirm the formation of a linear-nanoparticle structure upon the thermal cross-linking of the BCB units. Figure 1 shows the ^1H NMR of the diblock copolymer before and after the coil collapse for the samples containing 15% BCB. The peak at 3.10 ppm for the block copolymer belongs to the aliphatic protons of the benzocyclobutene group. This resonance peak completely disappeared after the thermal cross-linking reaction, replaced by a very broad resonance at 2.0–3.0 ppm. This is consistent with the ring-opening reaction of the benzocyclobutene units to give primarily the dibenzocyclooctane derivatives and higher aliphatic coupled oligomers.⁴⁶

Structural changes of the diblock copolymer after the thermal treatment at $250\text{ }^\circ\text{C}$ were investigated by GPC. This change is shown as a function of BCB content in Figure 2a. A systematic decrease in the hydrodynamic volume (or apparent molecular weight) of the total diblock copolymer is observed as a function of increasing BCB percentage. The percentage reduction in the apparent molecular weight obtained by the GPC trace scales with the increasing BCB content, as shown in Figure 2b.

It is possible to calculate the percentage reduction in the apparent molecular weight of the S-*r*-BCB block rather than the total molecular weight reduction, under the assumption that the hydrophilic PEG block of the diblock copolymer maintains its structure (and molecular weight of $20\,000$ g/mol) after the intramolecular collapse of the hydrophobic S-*r*-BCB block. The molecular weight reductions in the S-*r*-BCB blocks agree with the values obtained for the previously reported random copolymer of styrene and BCB nanoparticles by Harth et al.³⁶ For example, a nearly 70% reduction in the apparent molecular weight was reported for the polymer with 15% BCB and starting molecular weight of $44\,000$ g/mol. For the block copolymer studied here, the reduction in the apparent molecular weight was over 80% at the same cross-linking density. In addition, all GPC traces were symmetric. The absence of a shoulder at high M_w (at shorter retention time) indicates that no intermolecular cross-linking reaction

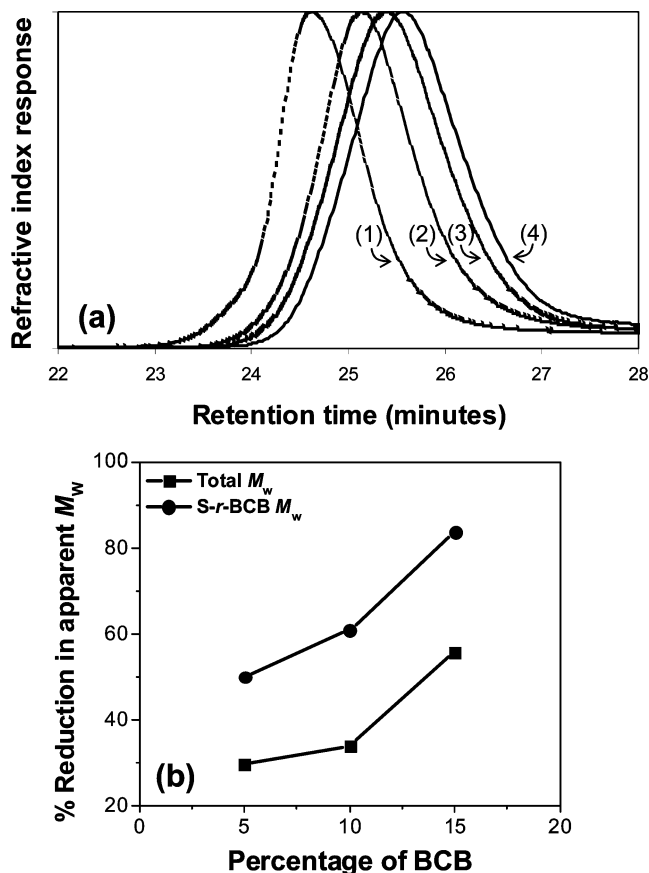


Figure 2. (a) GPC traces for (1) the starting linear block copolymer ($M_w = 64\,950$ g/mol, PDI = 1.16) and the resulting linear-nanoparticle block copolymers containing (2) 5 mol %, (3) 10 mol %, and (4) 15 mol % BCB. The lower plot (b) shows percent reduction in the apparent molecular weight of the block copolymer as a function of BCB percentage.

occurred during the nanoparticle formation and that the resulting polymer had a true single linear-nanoparticle structure without any intermolecularly cross-linked block copolymers. There was also no shoulder at low M_w (at longer retention time), verifying that the residual p(S-*r*-BCB) nanoparticle impurities had been removed by the cyclohexane extraction prior to the intramolecular cross-linking reaction.

Thermal Behavior of Bulk Systems. The thermal characteristics of the starting linear block copolymers and the linear-nanoparticle block copolymers resulting from intramolecular chain collapse are shown in Figure 3 and Figure 4. Two transitions were evident for all samples: an endothermic first-order transition corresponding to the melting of the PEG crystalline structure and a much smaller endothermic second-order transition corresponding to the glass transition of the amorphous S-*r*-BCB block. These two distinct thermal transitions were still observed after the coil collapse to form a linear-nanoparticle structure. Additionally, the nature of the cross-linking reaction (*intramolecular* vs *intermolecular*) and the architecture of the resulting systems (nanoparticle vs three-dimensional solid) were also investigated. Table 1 lists the melting temperatures (T_m of PEG), heats of fusion (ΔH_f of PEG), and glass-transition temperatures (T_g of S-*r*-BCB) of the linear block copolymer precursor and of the materials after intramolecular and intermolecular cross-linking of the precursor. The heats of fusion (measured from the area under the heat flow vs the temperature plot divided by the heating rate of the experiment) in Table 1 are reported as a value per total block copolymer, which

(46) Lloyd, J. B. F.; Ongley, P. A. *Tetrahedron* **1965**, *21*, 245.

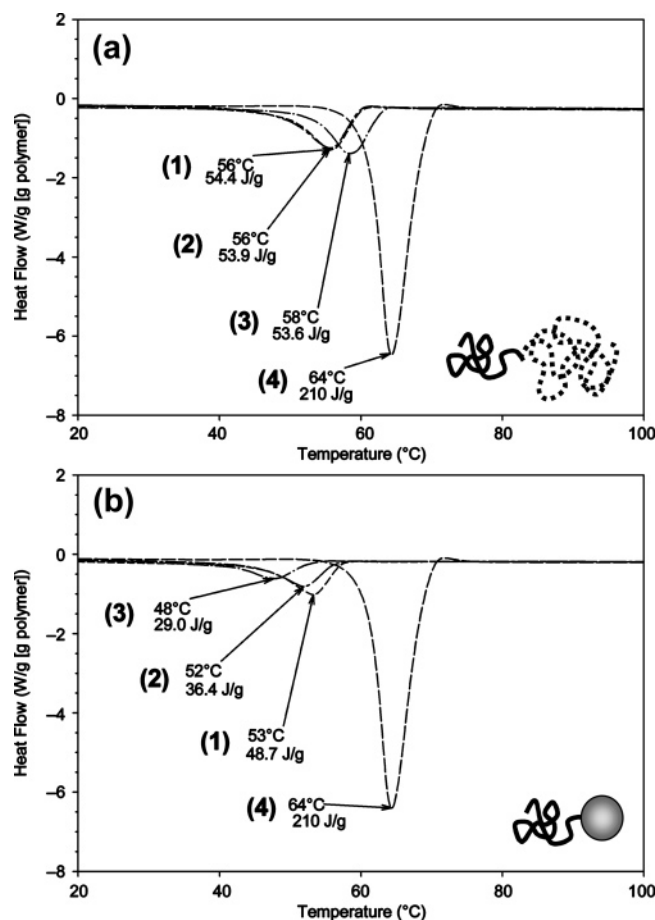


Figure 3. Heat flow vs temperature plot showing the melting transitions of the PEG block for (a) the linear and (b) the linear-nanoparticle block copolymers containing (1) 5 mol %, (2) 10 mol %, and (3) 15 mol % BCB. (4) Corresponds to the melting transition of monomethyl(poly(ethylene glycol)) ($M_w = 20\,000$ g/mol, PDI = 1.07). The melting temperature (°C) and the heat of fusion (J/g total block copolymer) are also listed.

includes both PEG and S-*r*-BCB blocks. For better comparison with the PEG homopolymer, the relative heat of fusion is calculated as follows for the PEG block by itself and is included in Table 1.

$$\text{relative heat of fusion (\%)} = \frac{\Delta H_{f, \text{block copolymer}}}{\Delta H_{f, \text{PEG homopolymer}}} \times \frac{\text{weight of total block copolymer}}{\text{weight of PEG block}} \quad (1)$$

The melting point temperature of the PEG block (56–58 °C) was depressed after the chain extension with the S-*r*-BCB block compared to that for the PEG homopolymer (64 °C), as seen in the heat flow versus the temperature plot (Figure 3a). Such melting point depression in PS-PEO diblock copolymers has been observed before.⁴⁷ It was also evident that the relative heat of fusion was decreased after the chain extension (64–72% for the linear block copolymers relative to 100% for the PEG homopolymer). These differences are consistent with the thermal behavior of the less compatible crystalline-amorphous block copolymers.⁴⁸ The melting point temperatures and the heats of fusion were similar among the linear block copolymers with varying BCB content, with the small

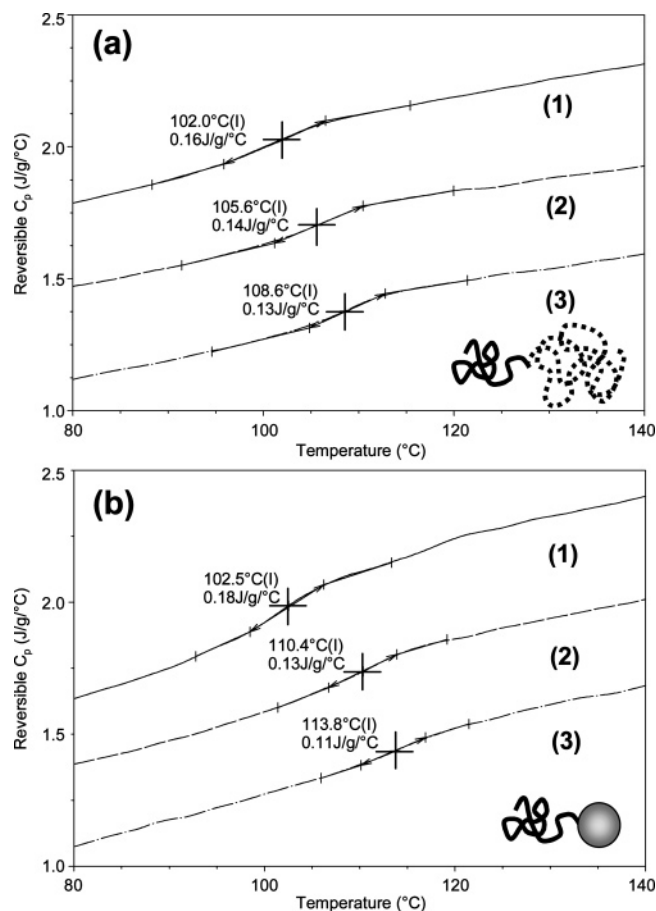


Figure 4. Reversible heat capacity vs temperature plot showing the glass transitions of the S-*r*-BCB block for (a) the linear and (b) the linear-nanoparticle block copolymers containing (1) 5 mol %, (2) 10 mol %, and (3) 15 mol % BCB.

differences being within the experimental error of the instrument (e.g., ± 2 °C for T_m).

After the intramolecular cross-linking of the S-*r*-BCB block (Figure 3b) to form the linear-nanoparticle block copolymers, there was a significant drop in T_m of the PEG crystalline structure, accompanied by a decrease in % relative heat of fusion, compared to the linear block copolymers. Moreover, the drops in T_m and % relative heat of fusion were significantly larger for the linear-nanoparticle block copolymer containing higher mol % BCB (Table 1).

T_g of the S-*r*-BCB block increased as the mol % of BCB in the second block was increased, both for the linear and for the linear-nanoparticle structures (reversible heat capacity vs temperature plot, Figure 4). In the case of the linear block copolymers, the T_g increase was small and the values of T_g were similar to that observed for polystyrene, which was ca. 100–105 °C ($T_g = 109$ °C for 15 mol % BCB, linear). By contrast, the increase in T_g for the linear-nanoparticle diblock copolymers was larger ($T_g = 114$ °C for 15 mol % BCB, linear-nanoparticle). This same behavior was also seen in the thermal response of the p(S-*r*-BCB) nanoparticles.³⁶

Figure 5 shows T_m (PEG block) and T_g (S-*r*-BCB block) as a function of the BCB mol % for the runs before and after heating the linear block copolymers up to 300 °C (corresponding to linear and intermolecular cross-linking, respectively) and the second run of the linear-nanoparticle block copolymers (corresponding to intramolecular cross-linking). The traces during the heating cycle up to 300 °C (not shown) for the linear block copolymers showed an

(47) Lotz, B.; Kovacs, A. *Polym. Prepr.* **1969**, *10*, 820–825.

(48) Unger, R.; Donth, E. *Acta Polym.* **1991**, *42*, 431–438.

Table 1. Melting Temperatures, Heats of Fusion, and Glass-Transition Temperatures of the Linear and Linear-Nanoparticle Block Copolymers as a Function of BCB mol %^a

mol % BCB	T_m (°C) of PEG block			ΔH_f (J/g) ^b (% relative to PEG homopolymer)			T_g (°C) of p(S- <i>r</i> -BCB) block		
	linear	intramolecular cross-linking	intermolecular cross-linking	linear	intramolecular cross-linking	intermolecular cross-linking	linear	intramolecular cross-linking	intermolecular cross-linking
5	56	53	55	54 (67)	49 (60)	54 (67)	102	103	116
10	56	52	54	54 (64)	36 (43)	54 (64)	106	110	134
15	58	48	57	54 (72)	29 (39)	54 (72)	109	114	161

^a The measurements are from the second runs for all samples. ^b Enthalpy of fusion per gram of total block copolymer.

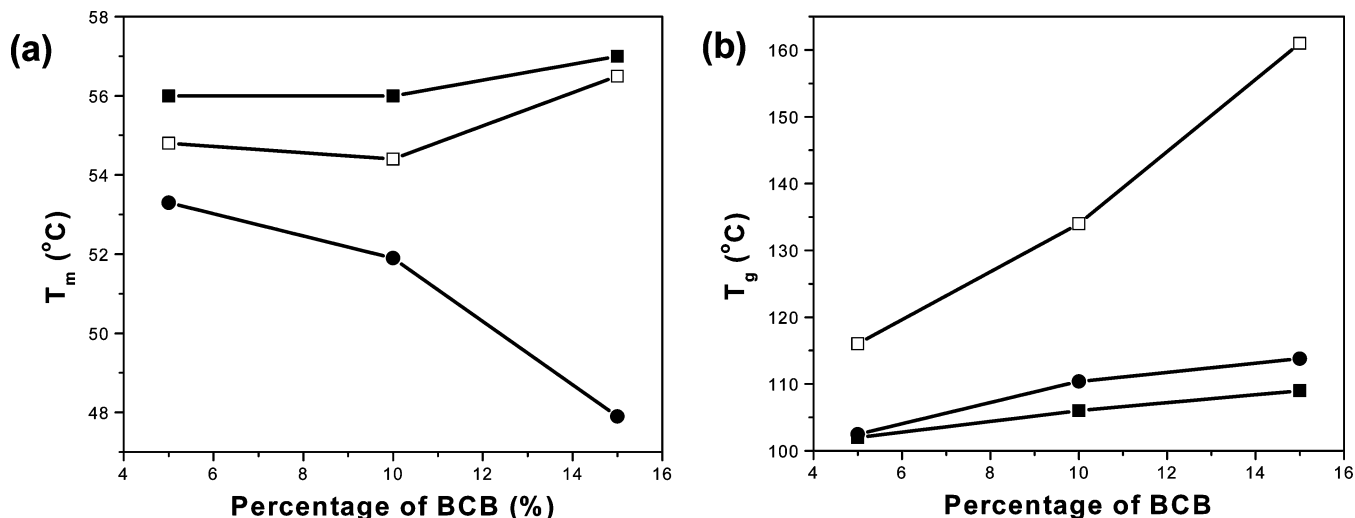


Figure 5. (a) Melting points of the PEG blocks and (b) glass-transition temperatures of the S-*r*-BCB blocks as a function of BCB percentage before (filled square, corresponding to linear block copolymer) and after (open square, corresponding to intermolecular cross-linking) heating the linear block copolymers up to 300 °C, and the second run (filled circle, corresponding to intramolecular cross-linking) of the linear-nanoparticle block copolymers.

exothermic transition near 250 °C corresponding to the ring-opening reaction of the cyclobutene units to give primarily cyclooctane derivatives. This reaction occurred in the bulk and therefore resulted in the intermolecular cross-linking of the BCB units and in a three-dimensional solid structure. The intermolecular cross-linking did not affect the melting transition of the PEG block, while the glass-transition temperature increased drastically.

Behavior at the Air–Water Interface. The π - A isotherms of the two different architectures are compared in Figure 6a–c for different cross-linking densities. Table 2 lists the limiting areas obtained from the isotherms, and the method by which they were determined is illustrated in Figure 6d.

The three linear block copolymers showed very similar compression isotherms, which have the characteristic features previously seen for PS–PEO diblock copolymers with relatively long PEO chains.⁴⁰ The isotherms had a slow increase in surface pressure at large molecular areas and exhibited a diffuse pseudo-first-order transition in the intermediate region, followed by a steep increase in surface pressure in the small molecular area regime. The isotherms of the linear block copolymers can be superimposed perfectly, except in the small molecular area region because of the slightly different molecular weights of the S-*r*-BCB blocks containing different mol % BCB.

The linear-nanoparticle block copolymers with different BCB mol % displayed similar isotherms in the very large molecular area region. However, there were several differences between the linear block copolymers and the linear-nanoparticle block copolymers and among the linear-nanoparticle block copolymers with different BCB contents. Compared to their linear counterparts, A_1 for the linear-nanoparticle structures was slightly smaller, Figure 6b, and this difference increased as a function of

increasing cross-linking density in the hydrophobic S-*r*-BCB block (Table 2). The length of the pseudoplateau was shorter for the linear-nanoparticle block copolymers compared to their linear counterparts.

The limiting area A_2 was larger and the increase in surface pressure after the pseudoplateau was at a higher molecular area (larger A_3) and was more gradual for the linear-nanoparticle structure containing more BCB units. Figure 7 makes the comparison in a plot of the superimposed isotherms of the linear-nanoparticle diblock copolymers. The molecular area at which collapse of the film occurs was smaller for the linear-nanoparticle block copolymer with higher cross-linking density.

Viscoelastic Properties at the Air–Water Interface. Viscoelastic properties of the linear and linear-nanoparticle block copolymers at the air–water interface were investigated as a function of surface pressure by measuring the dynamic moduli of the block copolymers at different states of compression. Frequency responses of the linear and linear-nanoparticle block copolymers containing 15 mol % BCB are shown in Figure 8 at different surface pressures along with the frequency response of a clean air–water interface.

For the linear block copolymer at relatively low pressures below the pseudoplateau pressure, the frequency-dependent measurement of the magnitude of the dynamic modulus, $|G_s^*(\omega)|$, agreed well with that of the clean air–water interface, indicating that the film behaved like a two-dimensional fluid at pressures below 8.0 mN/m. At higher surface pressures above the pseudoplateau region (i.e., 11.0 mN/m), abrupt changes in the behavior of the linear block copolymer were observed. The magnitude of the dynamic modulus was now constant as a function of frequency, or $|G_s^*(\omega)/\omega|$ decreased with increasing frequency. This “shear-thinning” phenomenon is character-

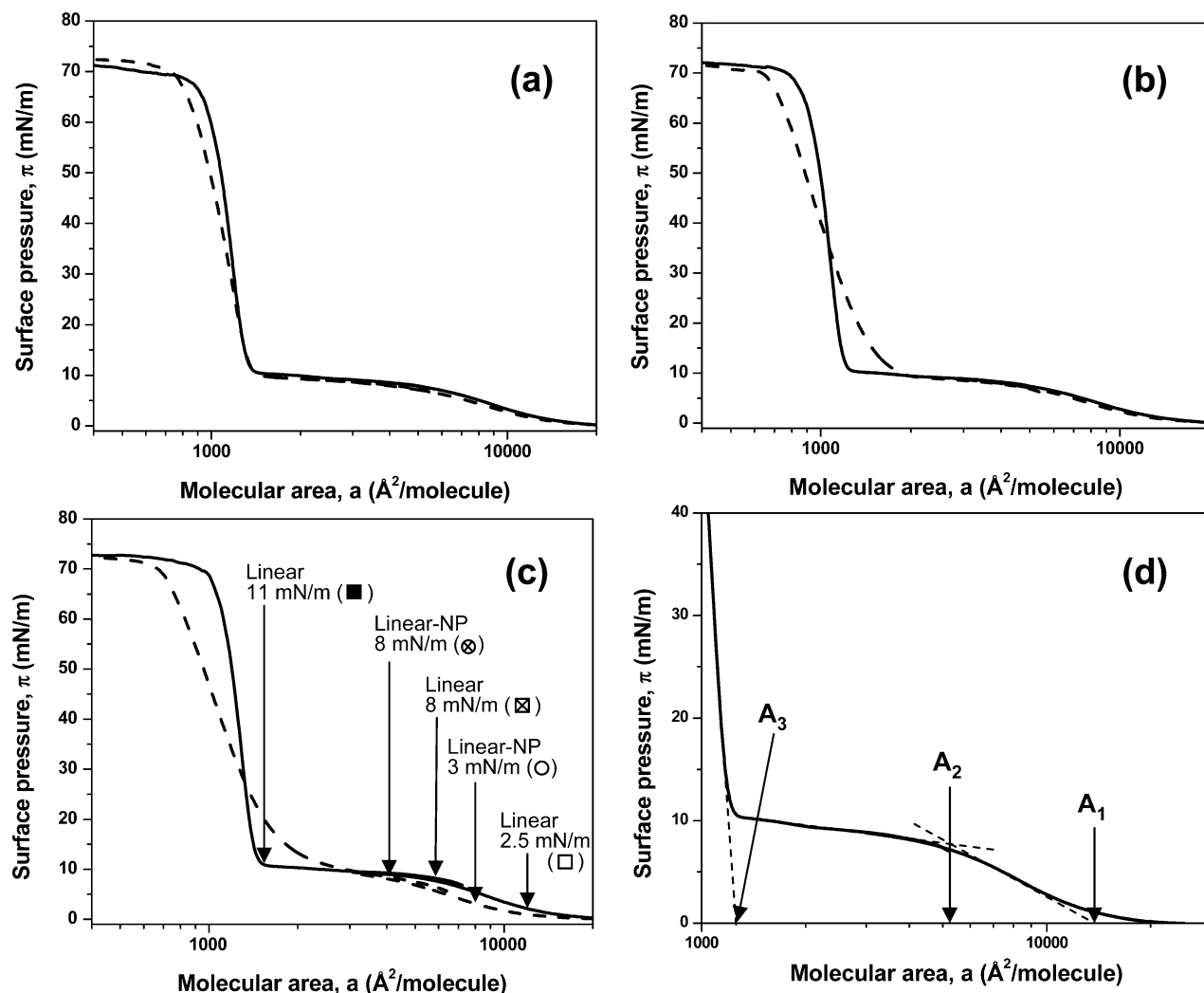


Figure 6. π - A isotherms of the linear (solid line) and linear-nanoparticle (dashed line) block copolymers with (a) 5 mol %, (b) 10 mol %, and (c) 15 mol % BCB. The isotherms were constructed from two compression experiments. The surface concentrations at which the ISR data in Figure 8 were taken are indicated in (c). The method by which the limiting areas were determined is shown in (d), and the limiting areas are tabulated in Table 2.

Table 2. Limiting Areas ($\text{\AA}^2/\text{molecule}$) of the Linear and the Linear-Nanoparticle Block Copolymers as a Function of BCB mol %^a

mol % BCB	linear ($\text{\AA}^2/\text{molecule}$)			linear-nanoparticle ($\text{\AA}^2/\text{molecule}$)			no. of EO (%) trapped in nanoparticle
	A_1	A_2	A_3	A_1	A_2	A_3	
5	14600	5530	1400	14000	5200	1500	18 (4.0%)
10	14600	5530	1260	13300	4920	1660	39 (8.6%)
15	14600	5530	1490	11300	4550	1970	100 (22%)

^a A_1 and A_3 were measured by extrapolation of the π - A isotherm to $\pi = 0$ mN/m. A_2 was determined at the crossing of the straight lines drawn along the large area and the intermediate regions of the isotherm.

istic of rubberlike materials and gels. Therefore, we observe a rheological transition from a liquidlike to a solidlike behavior, and this transition occurs over the surface pressure range that coincides with the pseudo-plateau region in the π - A isotherm of the linear block copolymer.

In the case of the linear-nanoparticle block copolymer, we observe the fluidlike behavior similar to that of the clean water surface only at a very low surface pressure (3.0 mN/m). We start to observe deviation from the waterlike behavior at a much lower surface pressure than for the linear block copolymer, and the behavior was already completely rubberlike at 8.0 mN/m (vs 11.0 mN/m for the linear block copolymer).

These differences between the linear and the linear-nanoparticle block copolymers were further explored when

their rheological properties were contrasted at different states of compression at a constant frequency of 1.0 rad/s. The storage (G_s') and loss (G_s'') moduli of the two architectures containing 15% BCB are plotted in Figure 9 as a function of surface pressure.

The abrupt increase in both G_s' and G_s'' of the linear block copolymer above 8.0 mN/m coincides with the transition in the π - A isotherm (pseudo-plateau), which occurs in the range of $\pi = 8$ -10 mN/m. For the linear-nanoparticle block copolymer, the increase in G_s' and G_s'' was smoother and started at a much lower surface pressure than 8.0 mN/m. While the response at low surface pressures for the linear block copolymer was independent of surface pressure up to the transition region (up to $\pi = 8.0$ mN/m), there was a constant increase in both G_s' and G_s'' for the linear-nanoparticle block copolymer in the same

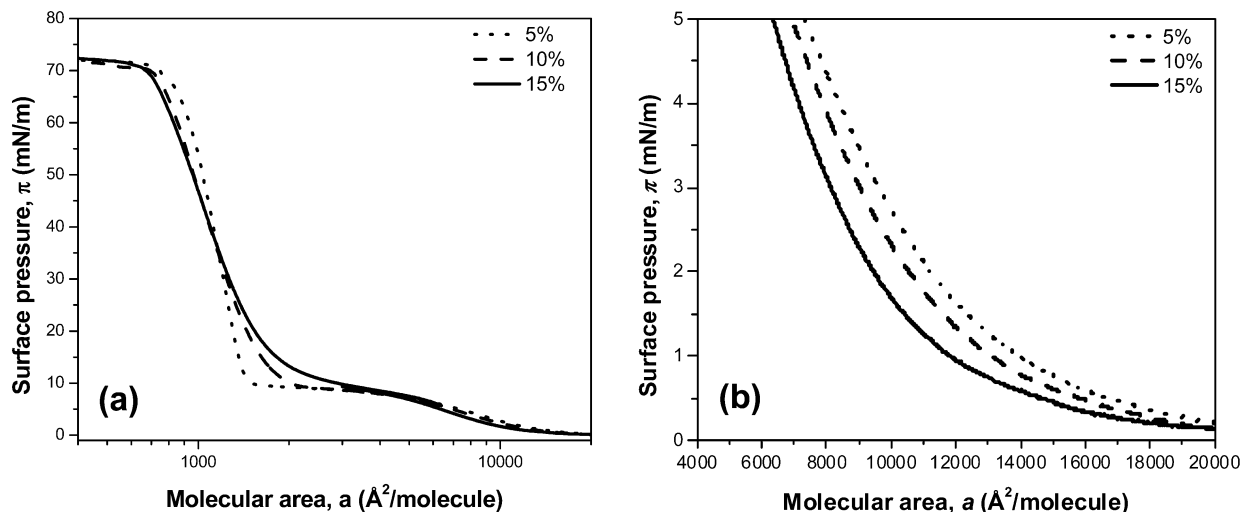


Figure 7. (a) π - A isotherms of the linear-nanoparticle block copolymers with different mol % BCB. The low surface pressure, or high molecular area region, is enlarged in (b).

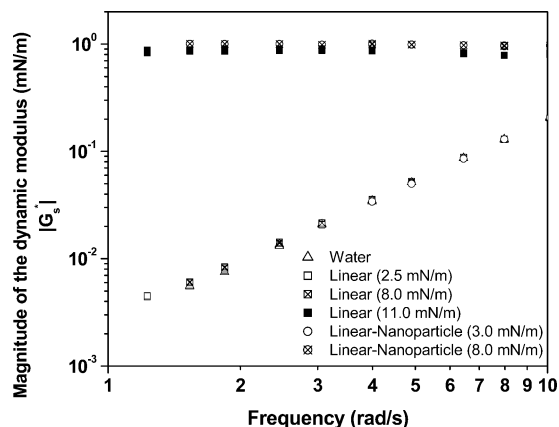


Figure 8. Frequency-dependent surface rheological measurements (magnitude of the dynamic modulus) at different surface concentrations as indicated in Figure 6(c). At low surface pressures, both linear and linear-nanoparticle block copolymers with 15 mol % BCB give the same fluidlike behavior as water. At a higher surface pressure, a rubberlike behavior is observed where $|G_s^*|$ stays constant as the frequency increases (shear-thinning behavior). This transition occurs at a much lower surface pressure for the linear-nanoparticle block copolymer (above 3 mN/m) than for the linear block copolymer (above 8 mN/m).

surface pressure region. A transition was also noticed for both block copolymers, from a liquidlike behavior where the loss modulus was larger than the storage modulus ($G_s' < G_s''$) to a solidlike behavior where $G_s' > G_s''$. This transition also occurred at a much lower surface pressure for the linear-nanoparticle block copolymer ($\pi = 3$ mN/m) than for the linear block copolymer ($\pi = 9$ mN/m). In addition, the magnitudes of both G_s' and G_s'' were much larger for the linear-nanoparticle block copolymer than for the linear block copolymer at $\pi > 3$ mN/m.

Langmuir-Blodgett Film Morphology. Indirect visualization of the block copolymer self-assembly was achieved by LB film transfer and subsequent imaging of the structures on the solid substrate by tapping mode AFM. Figure 10 shows the AFM images of the LB films at different surface pressures for the two architectures containing 15 mol % BCB. These images show surface aggregates rather than a smooth film, analogous to the aggregates of PS-PEO block copolymers reported earlier.^{9,11,49}

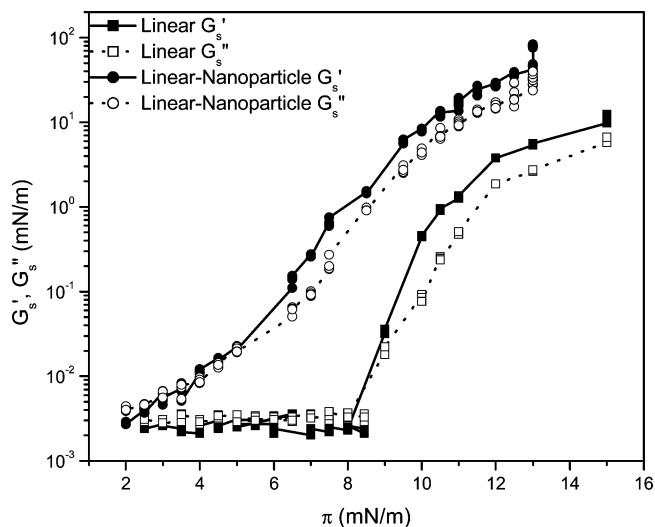


Figure 9. G_s' and G_s'' as a function of surface pressure for linear and linear-nanoparticle block copolymers containing 15 mol % BCB, measured at 1.0 rad/s. The lines are to aid the eye.

Two distinctly different interfacial morphologies were observed for the linear and the linear-nanoparticle block copolymers. The linear block copolymers formed disklike aggregates with relatively narrow size distribution throughout most of the isotherm, while the aggregates arising from the linear-nanoparticle block copolymers exhibited wormlike structures. At low surface pressures below the pseudoplateau region (< 8 mN/m), individual surface aggregates were observed for the disklike aggregates formed from the linear block copolymer. They started to pack more closely into little islands of disklike aggregates (of similar dimensions) at surface pressures above the pseudoplateau region (see enlarged image for 15 mN/m) and showed tightly packed structures at a higher surface pressure (see enlarged image for 25 mN/m). No multilayer structure was observed up to 25 mN/m. Close packing of the wormlike aggregates was also observed as a function of increasing surface pressure for the linear-nanoparticle block copolymers. The worms showed a random orientation below the short transition region, but signs of ordering were observed at higher surface pressures where the worms aligned themselves parallel to the

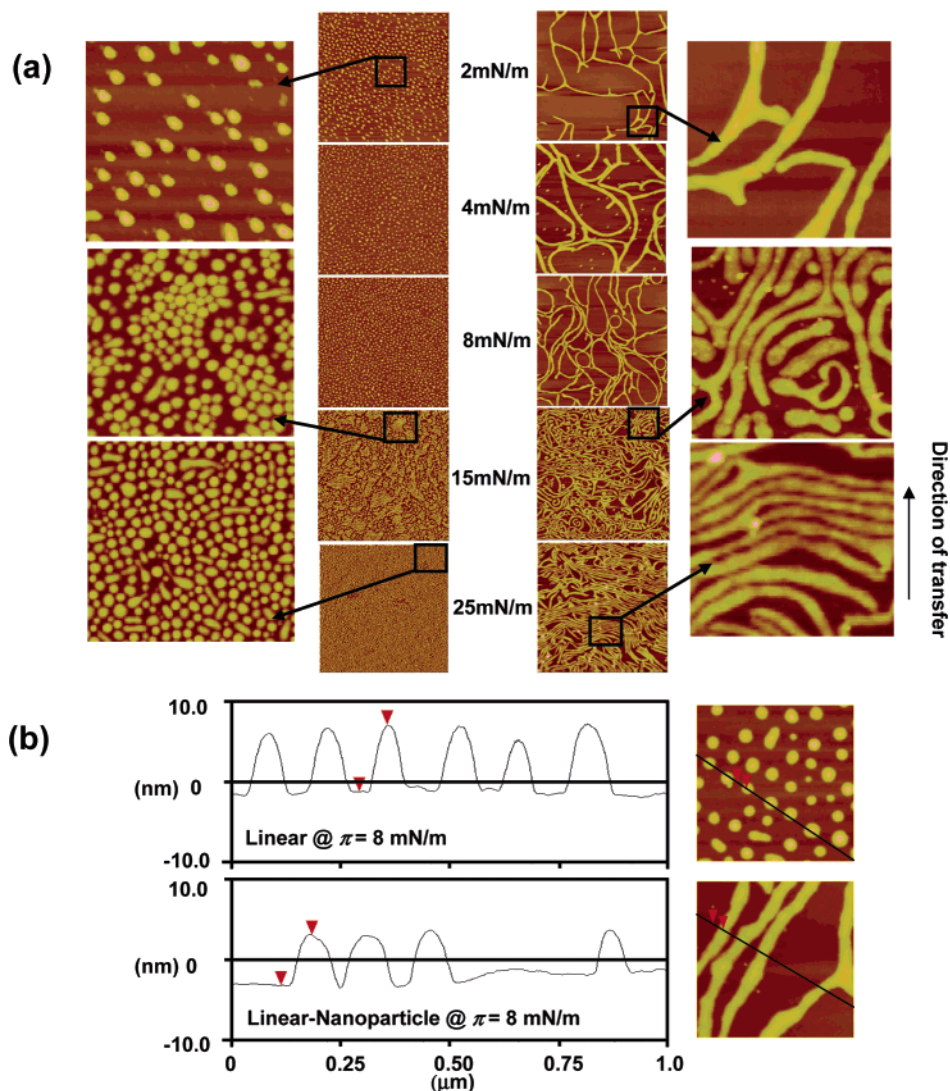


Figure 10. (a) AFM images of LB films transferred at different surface pressures. The left column shows films of the aggregates from the linear block copolymer and the right shows linear-nanoparticle block copolymer containing 15 mol % BCB. The horizontal scale is $5 \mu\text{m}$, and the vertical scale is 20 nm. The characteristics of the images are tabulated in Table 3. Enlarged images ($1 \mu\text{m} \times 1 \mu\text{m}$) are shown at 2, 15, and 25 mN/m. (b) Cross sections of the two different morphologies transferred at 8 mN/m. The average height of the surface aggregates is 8.0 ± 0.5 nm and 6.0 ± 0.5 nm for the linear and the linear-nanoparticle block copolymer aggregates, respectively.

Table 3. Characteristics of the LB Films as a Function of Surface Pressure^a

	π (mN/m)	transfer ratio	mean molecular area (\AA^2)	average diameter of p(S-r-BCB) domains (nm)	height (nm)	no. domains in $25 \mu\text{m}^2 (\pm 50)$	aggregation number ^b
linear	2	1.63	12 280	67 ± 16	8.0 ± 0.5	750	442
	4	1.55	9370	57 ± 21	8.0 ± 0.5	1060	391
	8	2.47	5500	63 ± 15	8.0 ± 0.5	1640	684
	15	0.73	1410	40 ± 13	8.0 ± 0.5	3680	352
	25	0.99	1340	44 ± 12	8.0 ± 0.5	5470	338
linear-nanoparticle	2	1.47	9470	60~80	6.0 ± 0.5		
	4	1.36	7120	60~80	6.0 ± 0.5		
	8	3.10	4490	60~80	6.0 ± 0.5	N/A	N/A
	15	0.90	1820	60~80	7.0 ± 0.5		
	25	0.82	1380	60~80	7.0 ± 0.5		

^a The aggregation number was calculated taking into account the transfer ratio. ^b The aggregation number was calculated by dividing the total number of molecules transferred onto the substrate by the total number of surface aggregates transferred. The total number of molecules was calculated by dividing the surface area of the substrate by the mean molecular area at the transfer surface pressure and multiplying this number by the transfer ratio.

barriers and perpendicular to the compression and transfer directions (see enlarged image for 25 mN/m).

The characteristics of the AFM images are tabulated in Table 3. The average diameter and the height of the disklike domains for the linear block copolymer stay

relatively constant as the surface pressure increases. It then follows that the aggregation number (N_{agg}) should also stay relatively constant as no coalescence of the aggregates was observed up to 25 mN/m, unlike the case of the three-arm star PS-PEO.²² However, there is some

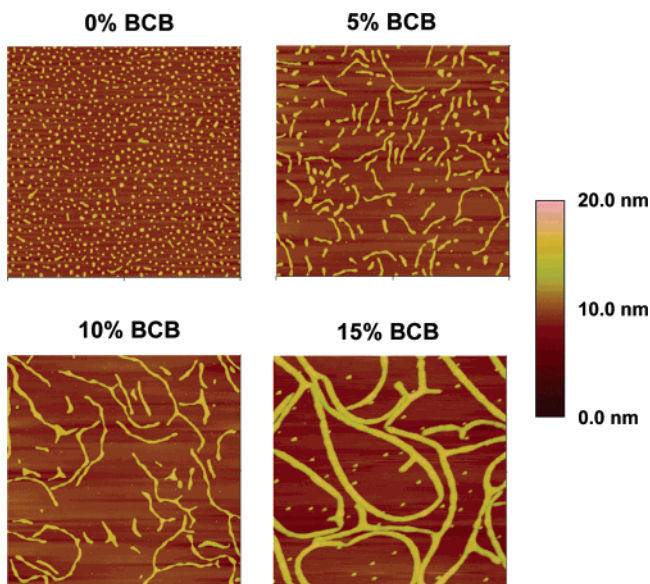


Figure 11. AFM images of LB films transferred at 4 mN/m for the linear block copolymer and the linear-nanoparticle block copolymers with different BCB content. The horizontal scale is 5 μm , and the vertical scale is 20 nm.

variation in the N_{agg} calculated at different surface pressures. The very large N_{agg} at 8 mN/m is not reliable since the transfer ratio reflected the especially large dilational creep near the pseudoplateau region. The aggregation numbers calculated at other surface pressures are more reliable since a very small dilational creep was measured at these surface pressures (i.e., <5% of the starting molecular area was lost after 1 h at 2 mN/m). As shown by the cross sections in Figure 10, the diameters of the two different aggregate structures corresponding to the two architectures were similar, but the height of the linear-nanoparticle diblock copolymer (6.0 ± 0.5 nm) was lower than that of the linear block copolymer (8.0 ± 0.5 nm).

The linear-nanoparticle block copolymers containing 5 and 10 mol % BCB exhibited very rich polymorphic transitions. Figure 11 shows the AFM images of linear-nanoparticle structures with different BCB mol % for LB films transferred at 4 mN/m. While the 15% BCB sample predominantly formed wormlike structures with occasional disklike aggregates, the other two samples containing fewer BCB units in the S-*r*-BCB block (thus, more loosely cross-linked than the 15% BCB sample) showed mixtures of disklike and wormlike aggregates. In addition, the length of the wormlike aggregates grew as a function of increasing BCB content or increasing number of cross-linked points. Wormlike structures longer than 10 μm were detected from the AFM images of the 15 mol % BCB containing linear-nanoparticle block copolymer. The heights of the aggregates of the 5 and 10 mol % BCB ranged 7.0 ~ 8.0 nm.

Discussion

Bulk Structure and Bulk Thermal Behavior.

Significant reduction in the hydrodynamic volume was seen by GPC after the thermal cross-linking of the BCB units in the S-*r*-BCB block of the block copolymer. This is consistent with the expected structural change of the S-*r*-BCB block from a random coil linear structure to a more compact globular structure of the nanoparticle. Higher cross-linking density in the S-*r*-BCB block produces block copolymers with smaller hydrodynamic volume, in line with the collapsed structure of a globular particle.

Comparison between the thermal behaviors of the linear and the linear-nanoparticle block copolymers reveals several interesting dynamic properties characteristic of the two different architectures. The crystallization of the PEG block is more extensively disturbed when the hydrophobic block undergoes intramolecular chain collapse than when it is a random coil. Furthermore, the change is larger for the block copolymer containing the nanoparticle with higher cross-linking density. This observation indicates that the block copolymer with more densely cross-linked nanoparticle block forms smaller or less crystalline PEG microdomains. This may be caused by altered microphase separation of the linear-nanoparticle block copolymer because of a reduced molecular mobility of the nanoparticle. The dynamics of the nanoparticle block are significantly hindered compared to the linear chain and, as expected, more densely cross-linked nanoparticles exhibited more rigid dynamics (higher T_g).

The nature of the cross-linking reaction significantly affects the resulting three-dimensional bulk structure. Intramolecular cross-linking yields linear-nanoparticle block copolymers that phase separate in the bulk, while intermolecular cross-linking produces a phase-separated three-dimensional solid with a more rigid network of cross-linked hydrophobic domains and the PEG crystalline domains that are similar to those in the linear block copolymer system. The T_g of the intermolecularly cross-linked system (161 $^{\circ}\text{C}$) is more than 50 $^{\circ}\text{C}$ higher than that of the starting linear block copolymer (109 $^{\circ}\text{C}$). The PEG crystalline domains are not affected by the intermolecular cross-linking, which essentially freezes in the rigid network of cross-linked hydrophobic domains phase-separated from the PEG domains. On the contrary, the PEG crystalline domains in the intramolecularly cross-linked system are affected by the nanoparticle block during the microphase separation and crystallization/melting processes, which is shown in the decreased T_m and relative heats of fusion of the PEG block.

For the bulk state structure of the linear-nanoparticle block copolymers, it is difficult to determine from the GPC results the impact of the intramolecular cross-linking of the hydrophobic block on the hydrophilic PEG chain of the block copolymer, because the individual hydrodynamic volumes of the two blocks cannot be distinguished. Fortunately, the π -*A* isotherms provide this information through the limiting molecular area A_1 , and we will discuss this effect shortly.

Structures at the Air–Water Interface: Discrete Molecule vs Surface Aggregate. In previous studies of linear PS–PEO block copolymers at the air–water interface, the presence of surface aggregates has been proposed when the study was combined with imaging of the resulting LB films that showed well-defined, quasi-two-dimensional⁸ surface aggregates.⁹ On the other hand, surface aggregates of other block copolymers have been detected in situ at the air–water interface. For example, off-specular X-ray reflection has been used to show that surface aggregates of a block copolymer of poly(styrene-*b*-pyridinium methyl iodide) are present at the air–water interface,⁵⁰ and Lin and co-workers⁵¹ used evanescent wave light scattering to measure the diameter of the disklike surface aggregates of poly(styrene-*b*-methyl methacrylate) system at the air–water interface. However, there have been no studies that investigated, in situ, the surface aggregation of a PS–PEO system spread at the

(50) Li, Z.; Zhao, M. W.; Quinn, J.; Rafailovich, M. H.; Sokolov, J.; Lennox, R. B.; Eisenberg, A.; Wu, X. Z.; Kim, M. W.; Sinha, S. K.; Tolan, M. *Langmuir* **1995**, *11*, 4785–4792.

(51) Lin, B. H.; Rice, S. A. *J. Chem. Phys.* **1993**, *98*, 6561–6563.

air–water interface from a solution, although Dewhurst et al.⁵² have reported the spontaneous adsorption of PS–PEO micelles from bulk aqueous solution to the air–water interface using specular neutron reflectometry, and the single drop experiment by Devereaux et al.¹² also showed the different morphologies resulting from aggregation on a solid substrate.

As a result, the PS–PEO π -A isotherm has routinely been interpreted under the assumption that individual discrete block copolymer molecules form a uniform film at the air–water interface. Using the grafted polymer theory,^{41,43} the different regions in the π -A isotherms have been attributed to pancake, quasi-brush (or mushroom), and brush conformations of the PEO chain for the PS–PEO block copolymers with long PEO chains.⁴⁰ However, the appropriate interpretation of the π -A isotherms would first require that the structure of the block copolymer at the air–water interface be known as a function of the compression state. If the presence of the surface aggregates at the air–water interface could be unambiguously confirmed by an in-situ experimental technique, the surface aggregates would have to be considered when interpreting the π -A isotherm. For example, by extending the three-dimensional micellization theory to the two-dimensional interfaces, Israelachvili⁵³ has shown that it is possible to construct and interpret a π -A isotherm in terms of the formation of surface micelles as a function of the increasing surface concentration because of compression.

We now use our surface viscoelastic property measurements of the PEG-*b*-p(S-*r*-BCB) block copolymers with different architectures at the air–water interface to elucidate the true block copolymer structure at the air–water interface. By combining these data and the AFM images of the LB transferred films of the block copolymers, we develop the appropriate interpretation of their π -A isotherms.

Viscoelastic Properties of Linear vs Linear-Nanoparticle Block Copolymers. The surface dynamic moduli are compared as a function of the surface pressure in Figure 9 for the linear and the linear-nanoparticle block copolymers containing 15 mol % BCB. Compared to the linear block copolymer, the linear-nanoparticle block copolymer showed significantly larger storage (G'_s) and loss (G''_s) moduli at all surface pressures. These results are examined below, assuming the two possible block copolymer structures at the air–water interface: discrete molecules and surface aggregates.

From the thermal analysis of the two polymers, we have already established that the nanoparticle formation through intramolecular cross-linking results in a much more rigid structure of the hydrophobic S-*r*-BCB block. However, at the experimental temperature of 25 °C, both the linear S-*r*-BCB chain and the nanoparticle S-*r*-BCB block are rigid globules at the air–water interface because their T_g 's are significantly higher than 25 °C. Therefore, discrete molecules of the linear and the linear-nanoparticle block copolymers are expected to show similar viscoelastic behaviors at the air–water interface at 25 °C. This is especially true at low surface pressures where the molecular interaction occurs largely between the PEG chains only. Thus, it is difficult to determine the source of the remarkably different behaviors of the two architectures if discrete molecules are assumed at the air–water interface.

Earlier, Naumann et al.⁵⁴ studied several PEG lipopolymers using the interfacial stress rheometer. The lipopolymers behave similarly to clean water surface well above (up to 17.5 mN/m) the pseudoplateau region (8–10 mN/m), showing very small dynamic moduli with low viscosity. The large S-*r*-BCB block anchoring our block copolymer to the interface may cause some differences in the viscoelastic behavior compared to the lipopolymers with small lipid anchors. If the pseudoplateau is ascribed to the transition of the PEG chain from a quasi-brush to a brush conformation, however, this difference is expected to be quite small, much smaller than the difference we observe between Naumann's lipopolymers and our linear block copolymer. Another possible cause for the very different rheological behaviors may be the different molecular weights of the PEG chains. The largest molecular weight of the PEG chain in the lipopolymers was only 5000 g/mol, much smaller than our 20 000 g/mol PEG chain. However, the PEG chain in our block copolymers is shorter than the critical molecular weight for entanglement ($M_w = 28\ 000$ g/mol), and thus, it is still difficult to explain the largely different rheological behaviors assuming discrete individual molecules of our block copolymer at the air–water interface.

Let us then consider the case in which the measured viscoelastic properties are those of the surface aggregates at the air–water interface rather than those arising from individual molecules. Here, we borrow from the rheological properties of three-dimensional surfactant solutions having different morphologies to understand our system. Disordered solutions of spherical micelles are not considered particularly viscoelastic or even viscous.⁵⁵ The solution only becomes viscous when the volume fraction of micelles becomes high, greater than 30 vol %. In contrast, rheology of dilute wormlike micellar solutions is complicated and it needs much work to understand many unusual phenomena occurring in these solutions.⁵⁵ Solutions with wormlike micelles usually become viscous at relatively low volume fractions compared to the spherical micelle solutions.⁵⁵

To understand the significant difference in the dynamic moduli of the two different block copolymer structures, we look at the experimental study⁵⁶ on the rheological properties of aqueous solutions of cetyltrimethylammonium chloride (CTAC) with salicylate as the binding counterion. The morphology of the cationic surfactant micelle is altered from spherical to wormlike geometry as the counterion concentration increases. As this morphological transition occurs, the solution is transformed from a low-viscosity Newtonian liquid to a highly viscoelastic solution. This observation is similar to the higher dynamic moduli of the wormlike aggregates of the linear-nanoparticle block copolymer and the waterlike behavior of the disklike aggregates of the linear block copolymer at low surface pressures or surface concentrations. The isotropic disklike surface aggregates of the linear block copolymer behave similarly to the clean water surface up to a much higher surface concentration compared to the anisotropic wormlike surface aggregates of the linear-nanoparticle block copolymer.

The sudden increases in both the storage and the loss moduli of the linear block copolymer coincide with the pseudoplateau observed in the π -A isotherm. Changes in

(54) Naumann, C. A.; Brooks, C. F.; Fuller, G. G.; Knoll, W.; Frank, C. W. *Langmuir* **1999**, *15*, 7752–7761.

(55) Larson, R. G. *The Structure and Rheology of Complex Fluids*; Oxford University Press: New York, Oxford, 1999.

(56) Clausen, T. M.; Vinson, P. K.; Minter, J. R.; Davis, H. T.; Talmon, Y.; Miller, W. G. *J. Phys. Chem.* **1992**, *96*, 474–484.

(52) Dewhurst, P. F.; Lovell, M. R.; Jones, J. L.; Richards, R. W.; Webster, J. R. P. *Macromolecules* **1998**, *31*, 7851–7864.

(53) Israelachvili, J. *Langmuir* **1994**, *10*, 3774–3781.

the morphology of the LB transferred disklike aggregates are seen before and after the pseudoplateau as well. Up to $\pi = 8.0$ mN/m, the LB transferred films show individual disklike aggregates without any evidence of coalescence. As the surface pressure increases, the distance between neighboring disklike aggregates decreases, showing closer packing of the aggregates. Since the small disklike aggregates exist as individual aggregates up to the pseudoplateau region, they may show the waterlike behavior at low surface pressures. However, above the pseudoplateau (at $\pi = 15.0$ mN/m), aggregation of the disklike aggregates into small islands is detected in the LB transferred films. Although complete coalescence into planar structures never occurs, this large-scale aggregation behavior may be the reason for the sudden change of the monolayer from a Newtonian liquid to a viscoelastic material.

Thus, we propose that the π - A isotherms of our block copolymers must include the surface aggregates, and such an interpretation is supported *ex situ* by the AFM images of the LB films and *in situ* by the preliminary measurements of the surface viscoelastic properties of the block copolymers at the air-water interface. We now examine the π - A isotherms in more detail incorporating the development of surface aggregates at the air-water interface.

π - A Isotherms. To interpret the π - A isotherm of our block copolymers, the correct mechanism of the surface aggregation must be known. Three different mechanisms have been proposed by which the block copolymer surface aggregates are formed at the air-water interface. In brief, they are (1) deposition of surface micelles in solution,⁴⁴ (2) compression-induced surface aggregation, and (3) spontaneous surface aggregation.⁹

When considering the surface aggregation of our block copolymers, it must be kept in mind that the surface aggregates are not at their thermodynamic equilibrium because of the high T_g of the *S-r*-BCB block. This aspect of the surface self-assembly is the reason that the resulting structures are termed aggregates rather than micelles and it is not appropriate to apply Israelachvili's treatment⁵³ of the surface micelles to construct the theoretical π - A isotherms for these aggregates. In solution, such structures are also referred to as "frozen" or "dead" micelles. The block copolymers studied here therefore form "quasi-" two-dimensional surface "aggregates" that resemble the traditional micelle morphologies. It also follows that the surface aggregates are not likely to be the result of the compression-induced aggregation alone because we observe the surface aggregates at surface pressures much lower than the plateau pressure corresponding to the critical micelle area in Israelachvili's two-dimensional π - A isotherm.

We believe that the spontaneous surface aggregation suggested by Cox et al.⁹ is the most probable source of surface aggregation of PS-PEO systems or our PEG-*b*-(*S-r*-BCB) block copolymers. Cox et al.⁹ have shown that the spreading solvent in the block copolymer solution has no effect in the morphology of the surface aggregates of PS-PEO, which indicates that the deposition of micelles in solution is an unlikely source of aggregation. In addition, they also showed that aggregation occurs prior to compression, through a TEM image of the spread film transferred at "zero" surface pressure, which precludes the compression-induced aggregation as a mechanism. Considering that our block copolymers are not at their thermodynamic equilibrium because of the high T_g of the hydrophobic block, surface aggregation is most likely to be a spontaneous process, which occurs upon deposition

of the block copolymer solution during the evaporation of the solvent.

The AFM images of the LB films in Figure 10 show that the concentration of the surface aggregates is relatively low at low surface pressures. The surface aggregates transferred at 2 mN/m showed large areas between the surface aggregates. From the phase images of the surface, there is very small contrast between the area corresponding to the aggregates and the spaces between the aggregates. A very large phase difference is expected if the spaces between the aggregates correspond to the bare Si(100) surface. Therefore, there is probably no bare surface between the surface aggregates. The distance between the aggregates, however, is too large to be occupied by the stretched PEG chains of the surface aggregates alone. We believe some individual molecules that have not aggregated into surface aggregates may occupy this space; however, we have no clear evidence for the presence or fraction of the individual molecules because of the difficulty of distinguishing the PEG and the *S-r*-BCB blocks in the AFM images, and it would need further investigation to determine what occupies the space between the aggregates that are not accounted for by the stretched PEG chains alone. As the surface pressure and the concentration of the aggregates increase, this space decreases. This may mean the transition of the aggregate conformation from the "starfish" to the "jellyfish", as was described by Zhu et al.⁸

Some support for the presence of a fraction of individual molecules at low surface pressures is provided by the aggregation numbers calculated for the surface aggregates of the linear block copolymer transferred at 2 mN/m and 4 mN/m. These values (442 and 390 at 2 mN/m and 4 mN/m, respectively) are slightly higher than those of the surface aggregates transferred at surface pressures above the pseudoplateau pressure (352 and 338 at 15 and 25 mN/m, respectively). Since the aggregation numbers are calculated assuming that all of the block copolymer molecules deposited at the air-water interface participate in the aggregation (see Table 3 for the method by which the aggregation number was determined), the calculated aggregation number would be larger than the actual number if some fraction of the deposited molecules in fact remained as discrete individual molecules at the air-water interface.

Previously, the onset of the surface pressure ($\pi > 0$ mN/m) in the π - A isotherms of PEO homopolymers, or PS-PEO block copolymers with large PEO/PS ratios, has been associated with the PEO pancake conformation. The corresponding limiting area (A_1 in Figure 6d) was earlier reported as 27–31 Å² per ethylene oxide (EO) repeat unit for the PS-PEO block copolymers containing 90–455 EO repeat units,⁴⁰ which was smaller than the values found for the PEO homopolymer (40–48 Å² per repeat unit).⁵⁷ For our linear block copolymers, this area (A_1) was found to lie between these values, at 33 Å² per repeat unit. The smaller molecular area at which the onset of surface pressure occurs for the block copolymers compared to the homopolymer also agrees with our picture in which a mixture of spontaneously formed surface aggregates and individual molecules exists at $\pi \approx 0$ mN/m.

We now propose the following to describe the surface aggregation of our block copolymers at the air-water interface. Upon deposition of the block copolymer solution at the air-water interface, the block copolymers spontaneously self-assemble into surface aggregates during the solvent evaporation. Upon compression, the stretched

(57) Sauer, B. B.; Yu, H. *Macromolecules* **1989**, *22*, 786–791.

PEG chains of the surface aggregates (in the “starfish” conformation) begin to interact with each other in their pancake conformation, giving rise to the surface pressure as described by the grafted polymer theory. The presence of the surface aggregates may be the reason that the onset of the surface pressure occurs at a limiting area smaller than the limiting area of the PEO homopolymer pancake conformation, as some fraction of the PEG chains lie underneath the aggregates.

For the disklike surface aggregates, the coalescence of tens of individual aggregates into small islands is observed at surface pressures corresponding to the pseudoplateau region ($8 \text{ mN/m} = \pi = 10 \text{ mN/m}$), which has been ascribed to the quasi-2D to 3D phase transition of the PEG chains by the grafted polymer theory. After the pseudoplateau, the surface pressure starts to increase again when the interaction becomes stronger such that the hydrophobic S-*r*-BCB blocks start to experience the repulsive interaction with the neighbors. The wormlike aggregates also become denser at higher surface pressures, but the π - A isotherms show almost no pseudoplateau (at 15 mol % BCB). This difference is explained in the discussion that follows below.

As the limiting area at $\pi \approx 0 \text{ mN/m}$ (A_1) reflects the size of the PEG chain in the pancake conformation, we can now investigate more closely the difference in the limiting area A_1 of the linear vs the linear-nanoparticle block copolymers. As shown in Table 2, the limiting area for the pancake conformation (A_1) of the PEG chains of the linear-nanoparticle block copolymers decreases as a function of increasing cross-linking density. This indicates that some fraction of the PEG chain showing a smaller limiting area A_1 may not be free to interact with the PEG chains of the neighboring block copolymers at the air–water interface. Entrapment of a fraction of the PEG chain could happen during the cross-linking reaction, which transforms the linear structure of the hydrophobic block into the collapsed structure of a nanoparticle. The PEG chain becomes trapped inside the nanoparticle as the nanoparticles form during the thermal cross-linking of the BCB units, whose reaction kinetics is very fast at 250 °C. The decrease in A_1 for the PEG pancake conformation results from a fraction of the hydrophilic PEG chain becoming entrapped in the nanoparticle block after the cross-linking reaction. Moreover, if we assume that each ethylene glycol (EG) repeat unit should occupy 33 \AA^2 of molecular area (A_1 for the linear block copolymers), the number of EG monomer units that must be trapped in the nanoparticle can be calculated as

$$\frac{A_1(\text{linear}) - A_1(\text{linear} - \text{nanoparticle})}{33 \text{ \AA}^2/\text{EG monomer}} \quad (2)$$

The results are included in Table 2.

Table 2 shows that a considerable number of PEG repeating units (22% for the 15 mol % BCB) are trapped inside the nanoparticle block as a consequence of the collapse of the S-*r*-BCB block. It is in some ways counterintuitive that the fraction of the trapped PEG chain is larger for the block copolymers with more compact nanoparticle structure. The more loosely structured nanoparticles containing smaller mol % BCB may be able to trap a greater fraction of the PEG monomer units than the more strongly cross-linked nanoparticles with larger mol % BCB. However, it is also likely that the trapped fraction of the PEG chain may reptate out of the loosely cross-linked structure more readily than from the tightly cross-linked structure when the hydrophilic PEG chain

encounters a good solvent such as chloroform. Thus, it follows that the portion of the irreversibly trapped PEG chain increases as the cross-linking density increases. The bulk structure of the individual linear-nanoparticle block copolymer molecule is then such that the length of the PEG chain is somewhat shorter than that of the starting linear block copolymer. This structural difference also explains the decrease of the pseudoplateau region for the linear-nanoparticle block copolymers having shorter PEG chains to undergo the quasi-2D to 3D phase transition.

As the surface aggregates are compressed further, the wormlike aggregates of the linear-nanoparticle structure eventually pack more compactly than the linear block copolymer, as is reflected in the smaller molecular area for the linear-nanoparticle block copolymers at the collapse pressure. Moreover, higher cross-linking density leads to the smaller molecular area at the collapse pressure, signifying the denser orientation of the long wormlike surface aggregates near the collapse pressure compared to the short wormlike aggregates arising from the less BCB containing linear-nanoparticle block copolymers (Figure 11).

LB Film Morphology and Surface Aggregates.

Surface aggregation of block copolymers is a rather general phenomenon and has been seen with block copolymers of PS containing various surface-active or surface-adsorbing blocks, both ionic and nonionic. Other than the PS–PEO systems,^{9,12,44} these include cationic blocks such as poly(vinylpyridine);^{6,50} neutralized anionic blocks such as poly(acrylic acid)¹⁷ and poly(methacrylic acid);¹⁷ or nonionic blocks such as poly(alkyl acrylates),¹⁴ poly(dimethylsiloxane),¹⁴ and poly(methyl methacrylate).^{19,20,51}

Self-assembly of these block copolymers at the air–water interface leads to “quasi” two-dimensional surface micelles or aggregates. They do not show truly two-dimensional microphase separation, as was seen with block copolymers containing two blocks that are both surface-adsorbing (e.g., poly(methyl methacrylate)-*b*-(octadecyl methacrylate)¹³). The amphiphilic block copolymers are anchored at the air–water interface by the hydrophobic block, while the hydrophilic block may become solvated and submerged into the subphase as the monolayer is compressed, assuming a jellyfish conformation.⁸ Therefore, these aggregates were previously described more correctly as quasi-2D aggregates.⁸

In this work, our main goal is to elucidate the effect of architecture on the surface self-assembly of block copolymers. The change of architecture from the linear chain configuration to the hybrid linear-nanoparticle arrangement results in differences in both structure and dynamics of the block copolymers, and these differences lead to the very different surface aggregate morphologies arising from the two architectures.

While the structural change due to intramolecular cross-linking results in vastly different geometries as seen by the GPC data, both the linear and the nanoparticle S-*r*-BCB blocks are expected to form glassy globules at the air–water interface at the experimental temperature, which is much lower than their T_g 's. Another change in the structure of the block copolymer because of intramolecular cross-linking occurs because a fraction of the PEG chain becomes trapped during the cross-linking reaction. In the case of the 15 mol % BCB containing block copolymers, it is shown that 22% of the PEG chain is trapped inside the nanoparticle after the intramolecular cross-linking. It is well-known that the relative sizes of the hydrophilic and hydrophobic blocks of the block copolymer play a very important role in determining the structure of surface aggregates. Cox et al.⁹ reported that

PS-PEO block copolymers containing below 66 mol % hydrophobic block (PS) formed disklike aggregates while those with larger hydrophobic blocks showed formation of wormlike aggregates (using block copolymers with total M_w between 14 000 and 27 000 g/mol).

Because part of the PEG chain is trapped inside the S-*r*-BCB nanoparticle in the linear-nanoparticle architecture, the PEG/S-*r*-BCB ratio is smaller for the linear-nanoparticle than for the linear architectures. The difference in the relative block sizes in the linear vs the linear-nanoparticle architectures indicates that the linear-nanoparticle block copolymer may have a greater tendency to form wormlike surface aggregates than the linear counterpart. If consideration is taken to include the fraction of the PEG block trapped inside the cross-linked S-*r*-BCB globule in the case of the linear-nanoparticle structures, we expect the contribution of the S-*r*-BCB block to increase up to 56 mol % for the 15% BCB containing sample (calculated assuming that 22% of the PEG block is considered part of the S-*r*-BCB block), 13 mol % higher than the linear precursor (43 mol % PS). Even after such consideration is taken, however, the linear-nanoparticle block copolymer is expected to form disklike, rather than wormlike, surface aggregates according to the experimental results by Cox et al.⁹ Thus, the effect of the trapped PEG chain in the S-*r*-BCB nanoparticle may not be the only source of the morphological change although the change occurs in such a way that the linear-nanoparticle architecture is more likely to form wormlike aggregates than the linear block copolymer.

We believe that there is another factor contributing to the morphology change beyond the shift in the block lengths because of entrapment of the PEG chain. This second factor has been recognized earlier in various studies involving micelle or aggregate formation of block copolymers in aqueous solution. In their 1996 paper,⁴⁹ Yu et al. studied the multiple morphologies of the PS-PEO aggregates in aqueous solutions and concluded that the main driving force for the morphological transitions is related to changes in the degree of stretching of the PS blocks in the core regions. A decrease in the soluble block length leads to a decrease in the entropy of the micelle core consisting of the same molecular weight insoluble block. When the entropy is decreased to a critical point because the insoluble block cannot be stretched further into the spherical micelle core, the spherical micelle structure becomes unstable and the morphology changes from spherical to nonspherical micelles such as cylinders or rods. Although the aggregate structures we observe with the LB transferred films of the PEG-*b*-p(S-*r*-BCB) diblock copolymers are two-dimensional surface aggregates rather than the three-dimensional aggregate structures in bulk aqueous solutions, the driving force behind the aggregation behavior is the same. During the solvent evaporation period when the block copolymers are allowed to rearrange themselves at the air-water interface, the cross-linked nanoparticle block has a much less degree of stretching to form the core of the disklike micelles compared to the linear S-*r*-BCB block. As a result, disklike micelles arising from the linear-nanoparticle block copolymers would have a void in the core of the aggregate, making the disklike morphology too unstable. Thus, the hybrid linear-nano-

particle architecture affects the geometrical packing of the molecules by decreasing the length of the PEG chain and lowering the degree of stretching of the insoluble nanoparticle block and leads to the nondisklike aggregate structure of the surface aggregates.

As a side note, the AFM image of the linear-nanoparticle structure transferred at 25 mN/m (Figure 10) showed a certain degree of alignment in a direction parallel to the barriers and perpendicular to the transfer direction. We have tried to improve the alignment by "annealing" the surface aggregates by repeated compression-expansion cycles. Although we were able to promote a coalescence of some disklike aggregates present at lower surface pressures (15 mN/m) into wormlike aggregates of more uniform thickness by this method (not shown), no significant improvement in the alignment of the worms was achieved.

Summary

We have presented a comparative study of PEG-*b*-p(S-*r*-BCB) amphiphilic block copolymers with the same molecular weights and chemical compositions but with different architectures. After the S-*r*-BCB block is thermally cross-linked to form a linear-nanoparticle structure, remarkably different bulk and surface properties are observed. The thermal behavior of the linear-nanoparticle block copolymer indicates more rigid dynamics of the nanoparticle block, and the hydrodynamic volume of the nanoparticle block is reduced by up to 80% compared to the linear chain. Markedly different surface aggregate morphologies are revealed from the AFM images of the LB transferred films of the two architectures: well-organized disklike aggregates are observed for the linear block copolymers, while long wormlike aggregates of up to 10 μm in length are seen for the linear-nanoparticle block copolymers. The hybrid linear-nanoparticle architecture also shows a surface viscoelasticity much higher than the linear block copolymer whose behavior is similar to clean water surface below the pseudoplateau pressure. The large differences in the surface viscoelastic properties of the two different architectures provide, for the first time, in-situ evidence of the block copolymer surface aggregation at the air-water interface, which has been supported only by the ex-situ AFM images of the transferred aggregates. The driving force for the different morphologies was found to be a combination of the change in the geometry of the block copolymer and the restricted degree of stretching in the nanoparticle block after the intramolecular cross-linking, thus emphasizing the effect of the architecture on the self-assembly process of these block copolymers.

Acknowledgment. We would like to thank Lucy Li and Ho-Cheol Kim, of IBM Almaden Research Center, for the modulated DSC data and thoughtful discussions regarding the AFM images, respectively. Financial support from the NSF GOALI program (Grant Number NSF CHE 9726146) and the NSF-MRSEC program (Award Number DMR-0213618) through the Center on Polymer Interfaces and Macromolecular Assemblies (CPIMA) is gratefully acknowledged.

LA047122F